

Enhancement of carrier mobility in thin Ge layer by Sn co-doping

Prucnal, S.; Liu, F.; Berencén, Y.; Vines, L.; Bischoff, L.; Grenzer, J.; Andric, S.; Tiagulskyi, S.; Pyszniak, K.; Turek, M.; Drozdziel, A.; Helm, M.; Zhou, S.; Skorupa, W.;

Originally published:

September 2016

Semiconductor Science and Technology 31(2016)105012

DOI: <https://doi.org/10.1088/0268-1242/31/10/105012>

Perma-Link to Publication Repository of HZDR:

<https://www.hzdr.de/publications/Publ-24338>

Release of the secondary publication
on the basis of the German Copyright Law § 38 Section 4.

Enhancement of carrier mobility in thin Ge layer by Sn co-doping

S. Prucnal^{1, a)}, F. Liu¹, Y. Berencén¹, L. Vines², L. Bischoff¹, S. Andric¹, S. Tiagulskyi^{1,3}, K. Pysznia⁴, M. Turek⁴, A. Drozdziel⁴, M. Helm¹, S. Zhou¹, W. Skorupa¹

¹*Institute of Ion Beam Physics and Materials Research, Helmholtz-Zentrum Dresden-Rossendorf, P.O. Box 510119, 01314 Dresden, Germany*

²*Department of Physics/Centre for Materials Science and Nanotechnology, University of Oslo, P.O. Box 1048 Blindern, N-0316 Oslo, Norway*

³*Lashkaryov Institute of Semiconductor Physics, National Academy of Sciences of Ukraine, Prospekt Nauki 41, 03028 Kiev, Ukraine*

⁴*Maria Curie-Skłodowska University, Pl. M. Curie-Skłodowskiej 1, 20-035 Lublin, Poland*

Abstract

We present the development, optimization and fabrication of high carrier mobility materials based on GeOI wafers co-doped with Sn and P. The Ge thin films were fabricated using plasma-enhanced chemical vapour deposition followed by ion implantation and explosive solid phase epitaxy, which is induced by millisecond-range flash lamp annealing. The influence of the recrystallization mechanism and co-doping of Sn on the carrier distribution and carrier mobilities both in the n-type and in the p-type GeOI wafers is discussed in details. This finding significantly contributes to the state of the art of high carrier mobility-GeOI wafers since the results are comparable with GeOI commercial wafers fabricated by epitaxial layer transfer or Smart Cut technology.

Keywords: GeOI, flash lamp annealing, explosive recrystallization, doping, ion implantation

^{a)}Electronic mail: s.prucnal@hzdr.de

Introduction

The incorporation of different functional optoelectronic elements into a single chip enables performance progress, which can overcome the downsizing limit in silicon technology. For example, the use of Ge instead of Si as a basic material in nanoelectronic would enable faster chips containing smaller transistors [1-3]. The efficient and cost-attractive integration of Ge with silicon technology for the future high-speed optoelectronics can be done using only a thin Ge layer placed on cheap substrates. In order to fully exploit the unique optoelectronic properties of Ge, the GeOI and Ge-on-Si structures have to be explored.

Another issue, which has to be addressed before the high performance Ge based nanoelectronics could be created, is the fabrication of highly-doped p- and n-type ultra-thin Ge layers and Ge nanostructures. In general, it has been shown that the n-type doping of Ge is a key bottleneck in the realization of advanced NMOS device performance [4]. According to the Roadmap 2013 for the next generation nanoelectronics, the device architecture should focus on the non-planar FETs using nanowire- or fin-based architectures [5]. Since the diffusion process in semiconductors is difficult to be precisely controlled, the ion implantation followed by ultra-short annealing e.g. in the millisecond range (ms-range) might be the alternative to achieve high-mobility channel materials in nanoscale. Over last years, ms-range flash lamp annealing (FLA) was successful applied for the fabrication of Si-based light emitting devices [6], ultra-shallow junction formation [7], recrystallization of SiC [8] and integration of III-V compound semiconductors with Si technology [9, 10]. Here we expand the application of ms-range FLA into Ge which will enable its full integration with large-scale silicon technology.

The carrier mobility and optical band gap in Ge can be engineered via Sn alloying and strain [11, 12]. The fabricated GeSn alloy films show the direct optical band gap for Sn concentration above 8% [13]. To this day, the GeSn films are mainly made by deposition techniques like molecular beam epitaxy and chemical vapour deposition [13, 14]. But GeSn alloy can be also fabricated by Sn implantation into a Ge film and post-implantation non-equilibrium thermal processing like nanosecond pulsed laser annealing (PLA) [11].

In this paper we present a successful fabrication of polycrystalline GeOI structure by deposition of amorphous Ge film on insulator and recrystallization during ms-range FLA. The optoelectronic properties of Ge film were modified by Sn and P co-implantation. Sn and P are incorporated into Ge films by ion implantation followed by ms-range explosive solid phase

epitaxy during the FLA process. It is shown that Sn co-doping significantly enhances both electron and hole mobility. Moreover, the lattice parameter of the fabricated films strongly depends on co-doping, which increases after alloying with Sn and in turn is partially compensated by P co-doping.

Experimental part

50 nm-Ge thin film was deposited on the 4 inch Si wafer covered with 150 nm of insulating layer (50 nm of SiO₂ and 100 nm of Si₃N₄) using plasma-enhanced vapour deposition (PECVD) technique. Subsequently, 50 nm-Si₃N₄ capping layer was deposited on the top in order to protect the Ge layer from contamination during ion implantation and annealing processes. Both the Ge and the Si₃N₄ layers were deposited at 300 °C, which ensures the amorphous Ge layer formation. Since the gas precursors for the Ge and Si₃N₄ deposition contain hydrogen (GeH₄ for Ge deposition and SiH₄ + NH₃ for Si₃N₄) it is expected that the deposited films are hydrogenated. The recrystallization and partial dehydrogenation of deposited films take place during ms-range FLA. The FLA was performed for 3 or 20 ms. Prior to the ms-range recrystallization, samples were implanted with Sn and P in order to modify the electronic and microstructural properties of GeOI films. Sn and P were implanted with fluences of $2 \times 10^{15} \text{ cm}^{-2}$ and $1 \times 10^{15} \text{ cm}^{-2}$, respectively. The ion energy was 150 keV for Sn and 50 keV for P. The microstructural properties of undoped and doped GeOI:Sn structures were investigated by means of X-ray diffraction (XRD) and electron backscattering diffraction pattern (EBSD). For EBSD a Bruker QUANTAX EBSD system on a Zeiss NVision40 crossbeam was used with electron beam energy of 20 keV. XRD was performed by an Empyrean Panalytical diffractometer with a Cu-target source. The setup is equipped with a Göbel mirror and an asymmetric monochromator to enhance the brilliance and monochromaticity. Moreover, the strain accumulation and recrystallization of GeOI:Sn films were studied by μ -Raman spectroscopy in backscattering geometry in the range 100 - 700 cm⁻¹ using a 532 nm Nd:YAG laser with a liquid-nitrogen cooled charge-coupled device camera. The electrical properties of fabricated films were investigated by means of Hall Effect measurements using Van der Pauw method. Dopant concentration versus depth profiles were measured by time-of-flight secondary ion mass spectrometry (ToF-SIMS) employing a Cameca IMS7f micro-analyzer. A beam of 15 keV Cs⁺ ions was rastered over a surface area of 200×200 μm^2 and secondary ions were collected from the central part of the sputtered crater. Crater depths were measured with a Dektak 8 stylus profilometer, and a constant erosion rate was assumed when converting sputtering time to sample depth.

Results and discussion

The microstructural properties of the deposited and implanted Ge thin films on insulator were analyzed by XRD. Figure 1 shows the XRD pattern of the fabricated GeOI films after ion implantation of Sn and/or P followed by FLA for 3 ms at 55.6 Jcm^{-2} . The XRD pattern from the as-deposited sample is also shown. The as-implanted sample shows only very broad peaks at about 25 and 50 of 2θ deg indicating an existence of amorphous, or at least, strongly disordered material. This fact is expected since the deposition temperature was lower than the recrystallization temperature for undoped Ge ($300 \text{ }^\circ\text{C}$).

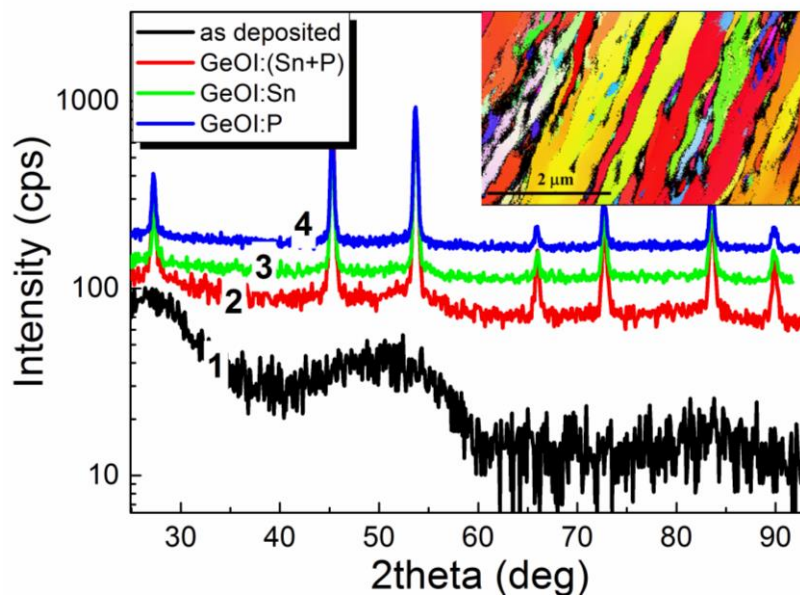


Figure 1. XRD pattern recorded from as-deposited and implanted GeOI after FLA at 55.6 Jcm^{-2} for 3 ms (1-as deposited, 2-GeOI doped with Sn and P, 3-GeOI doped with Sn only and 4-GeOI doped with P only). The inset shows the EBSD image ($2 \times 4 \text{ } \mu\text{m}^2$) of P doped GeOI. XRD curves were shifted vertically for clarity.

Curves 2 to 4 (see Fig. 1) show the XRD patterns obtained from implanted and annealed samples. The observed X-ray reflection peaks prove the formation of poly-crystalline Ge films. Moreover, the intensity ratio between every single peak and the intensity of reflection along (111) follows the rules for powder-like sample. Next, the average grain size and the lattice parameter of implanted Ge were extrapolated from XRD data. The obtained values are summarized in Table 1. The smallest lattice parameter was measured for Ge layer doped with P ($a_p = 5.573 \pm 0.005 \text{ \AA}$). The effective ionic radius of P is smaller than the radii of Ge (106 pm for P vs. 122 pm for Ge). This causes the biaxial lattice compression. Therefore, the highly P-doped Ge is expected to have the smallest lattice parameter and thus a slight shift of XRD

pattern towards lower 2θ value is observed. On the other hand, the Sn atoms are much bigger than Ge (141 pm for Sn). This causes an increase of lattice parameter up to $a_{\text{Sn}}=5.671\pm 0.005$ Å. Additionally, due to partial strain compensation by P the double implanted Ge film (Sn+P) reveals a lattice parameter slightly smaller than that of sample solely doped with Sn.

Table 1. Average lattice parameter, distortion parameter and ion fluence of annealed GeOI. The lattice parameter of relaxed crystalline Ge is $a=5.658$ Å.

| | Ion fluence | Lattice parameter (a) | Distortion (ϵ) |
|-----------|---|-----------------------|---------------------------|
| GeOI:P | 1×10^{15} cm ⁻² | 5.573 ± 0.005 Å | -1.50% |
| GeOI:Sn | 2×10^{15} cm ⁻² | 5.671 ± 0.005 Å | 0.23 % |
| GeOI:Sn+P | 2×10^{15} cm ⁻² + 1×10^{15} cm ⁻² | 5.668 ± 0.005 Å | 0.17 % |

Having lattice parameter for undoped fully relaxed crystalline Ge ($a_0=5.658$ Å) and the lattice parameters of the fabricated sample, it is possible to estimate the relative distortion (ϵ) within the recrystallized Ge layer according to following relationship:

$$\epsilon = \frac{a_{\text{exp}} - a_0}{a_0} \quad (1)$$

where a_{exp} and a_0 are the experimentally obtained and the tabulated lattice parameter values of Ge, respectively. Negative distortion suggests a compressively strained layer along the growth direction while a positive ϵ refers to the tensile strain. The obtained distortion parameters for fabricated GeOI are summarized in Table 1. The inset of Fig. 1 shows the EBSD image of P implanted and annealed GeOI sample. In close agreement with standard XRD pattern results, the EBSD investigation confirms the polycrystalline Ge film formation. The average size of the Ge crystals is few micrometres long and 200 nm width. The shape and size of crystals visualised by EBSD suggest that the recrystallization of 50 nm Ge thick films is mostly due to the explosive solid phase (ESP) recrystallization in the millisecond timescale [14-17]. Neither the XRD pattern nor EBSD shows any surface preferential orientation. This means, unfortunately, that the control of the grain orientation during ESP process would be challenging.

The crystallinity of implanted and annealed GeOI was further cross-checked by the micro-Raman spectroscopy. Figure 2 shows normalized Raman spectra obtained from implanted and annealed samples. The main peak corresponding to the transversal optical (TO)/ longitudinal optical (LO) phonon mode in single crystalline Ge is expected to be at about 300.5 cm⁻¹ [18].

Here the TO/LO phonon mode peak position is shifted towards lower wavenumbers, which is located at 297.6 for P doped sample, at 296.3 cm^{-1} for double implanted GeOI and at 296.0 cm^{-1} for Sn doped only, respectively (see Fig. 2). The shift of the main phonon mode towards lower wavenumbers is ascribed to the polycrystalline nature of recrystallized Ge thin film and it is mainly caused by the formation of strained layer during the recrystallization process and quantum confinement phonon effect [19].

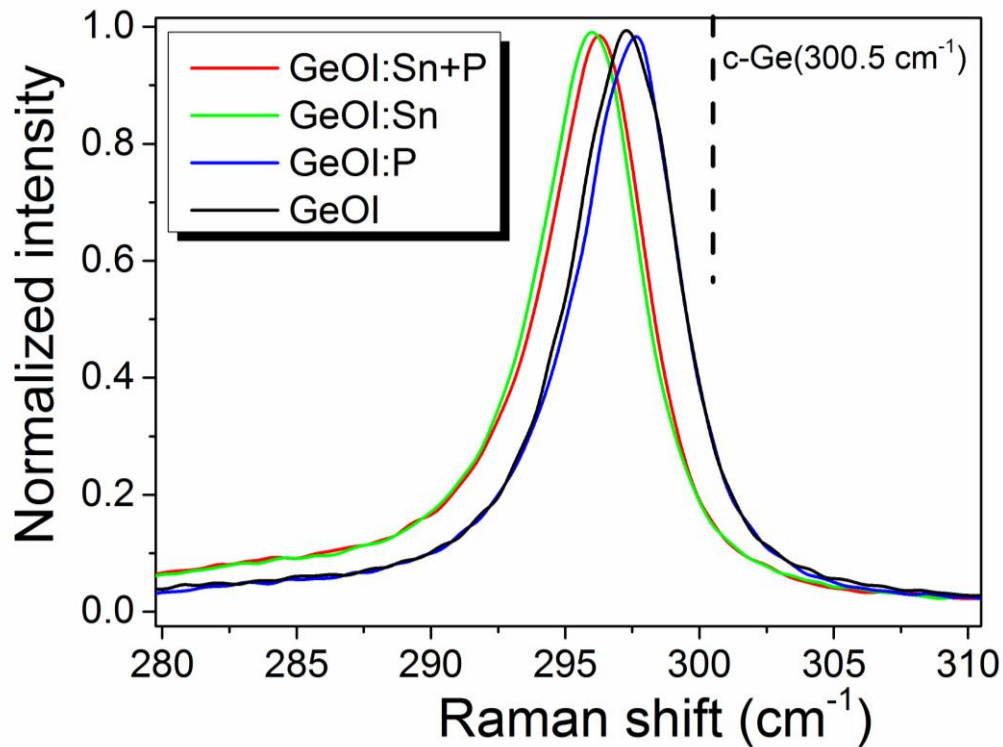


Figure 2. Micro-Raman spectra obtained from the undoped GeOI sample and GeOI samples implanted with Sn and P followed by FLA for 3 ms at 55.6 Jcm^{-2} . The peak position of the TO/LO phonon mode in bulk Ge is marked with a dashed vertical line.

The general behaviour of presented micro-Raman spectra is consistent with XRD data. The biggest shift towards lower wavenumbers indicates the biggest strain and/or existence of the crystal structure with the biggest lattice parameter. Taking into account the XRD data and the structural composition of GeOI layers, we can conclude that the shift of the phonon mode in Raman spectra is due to effect of quantum confinement on phonons and GeSn alloy formation, which is partially compensated by P co-doping.

The electrical properties of GeOI wafers were investigated by Hall Effect measurements. The obtained values are listed in Table 2. Similar to the undoped GeOI, GeSn alloy shows p-type

conductivity, but with an average carrier concentration in the range of $8 \times 10^{18} \text{ cm}^{-3}$ and carrier mobility of around $140 \text{ cm}^2 \text{ V}^{-1} \text{ s}^{-1}$. Both values are almost one order of magnitude higher than those of the undoped GeOI layer annealed by the same condition.

Table 2 – Room-temperature carrier concentration and carrier mobility for undoped and implanted GeOI wafers after annealing obtained by Hall Effect measurements.

| | Annealing parameters | Conductivity type | Carrier concentration | Carrier mobility |
|-----------|-------------------------------|-------------------|--------------------------------------|--|
| GeOI | 3 ms, 55.6 Jcm^{-2} | <i>p-type</i> | $1.1 \times 10^{18} \text{ cm}^{-3}$ | $12 \text{ cm}^2 \text{ V}^{-1} \text{ s}^{-1}$ |
| GeOI | 20 ms, 120 Jcm^{-2} | <i>p-type</i> | $8.1 \times 10^{17} \text{ cm}^{-3}$ | $45 \text{ cm}^2 \text{ V}^{-1} \text{ s}^{-1}$ |
| GeOI:P | 3 ms, 55.6 Jcm^{-2} | <i>n-type</i> | $1.1 \times 10^{19} \text{ cm}^{-3}$ | $74 \text{ cm}^2 \text{ V}^{-1} \text{ s}^{-1}$ |
| GeOI:Sn | 3 ms, 55.6 Jcm^{-2} | <i>p-type</i> | $8.4 \times 10^{18} \text{ cm}^{-3}$ | $138 \text{ cm}^2 \text{ V}^{-1} \text{ s}^{-1}$ |
| GeOI:Sn+P | 3 ms, 55.6 Jcm^{-2} | <i>n-type</i> | $2.5 \times 10^{19} \text{ cm}^{-3}$ | $130 \text{ cm}^2 \text{ V}^{-1} \text{ s}^{-1}$ |

It is known that most of defects like the Ge vacancies (V) and Ge interstitials have energy levels close to the valence band edge. They are responsible for the p-type conductivity of non-intentionally doped Ge [19]. Moreover, hydrogen is known as shallow acceptor in Ge with an activation energy below 20 meV [20]. Therefore, in undoped samples both defects and H impurities are responsible for the p-type conductivity. In our case, Ge layers were deposited by PECVD with GeH_4 molecules as the source of Ge. Hence, the Ge films were naturally contaminated with hydrogen. In addition, the Si_3N_4 capping layer hinders the out-diffusion of H during the recrystallization process, while the insulator layer below Ge acts as the extra source of H. The H depth distribution along the Ge films after different fabrication steps (deposition, implantation and annealing) is shown in Fig. 3. Prior the ToF-SIMS measurements the Si_3N_4 capping layer was removed by wet chemical etching in phosphoric acid. As can be seen (in Fig 3), H is quite homogeneously redistributed over the Ge film thickness. Only in the as-deposited stage an abrupt increase of H concentration is observed at the Ge- Si_3N_4 interface. The accumulation of H at the Ge-SiN interface is due to out-diffusion of H from the Si_3N_4 layer during Ge deposition. In general, the H concentration in PECVD-obtained layers strongly depends on the deposition temperature and the diffusion coefficient of H. According to SIMS measurements, the Si_3N_4 layer deposited at $300 \text{ }^\circ\text{C}$ contains about 10 % of H. During both ion implantation and the next annealing step, a slight redistribution of

H in our GeOI takes place. The most pronounced decrease of H content occurs at the Ge/Si₃N₄ interface while the H concentration remains constant over the Ge layer.

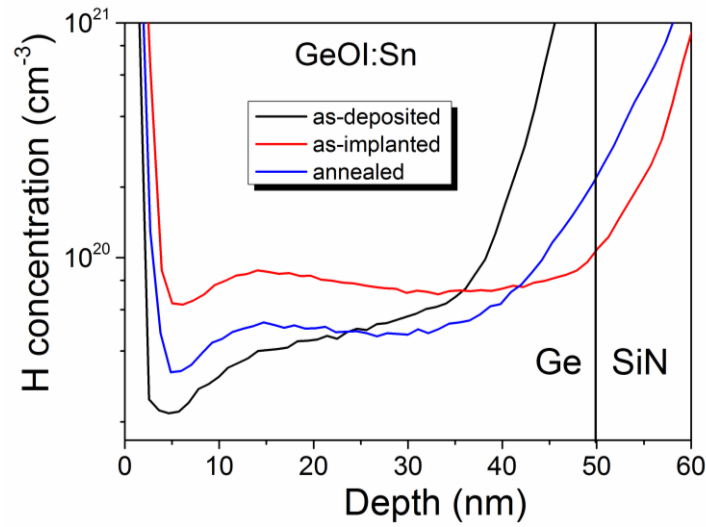


Figure 3. Hydrogen depth distribution in the GeOI sample at different fabrication steps obtained by ToF-SIMS. The sample was implanted with Sn and flash lamp annealed for 3 ms with an energy of 55.6 Jcm⁻².

P implanted and subsequently annealed by FLA GeOI shows n-type conductivity due to electrical activation of P atoms. Sample implanted only with P shows a carrier concentration in the range of $1.1 \times 10^{19} \text{ cm}^{-3}$, whereas a maximum electron concentration ($n_e = 2.5 \times 10^{19} \text{ cm}^{-3}$) was measured for the double implanted samples (Sn+P). Likewise, the carrier mobility was found to be $74 \text{ cm}^2\text{V}^{-1}\text{s}^{-1}$ for P implanted GeOI layers and almost twice higher for Sn+P implanted GeOI ($130 \text{ cm}^2\text{V}^{-1}\text{s}^{-1}$). This suggests an improvement of crystallinity of Ge layer by alloying with Sn as well as an effective reduction of defects. The most plausible explanation is that Sn deactivates some of defects by the formation of Sn-V complex which significantly decreases the concentration of scattering centers (mobility enhancement) and in turn the compensation of electrons [21]. Moreover, the strain engineering in Ge thin layer via Sn alloying may have also positive influence on the carrier mobility. Figure 4 shows the comparison between our best obtained results and single crystalline GeOI made by Smart Cut and epitaxial layer transfer method [22, 23]. In the case of n-type GeOI, the epitaxial Ge and GeOI made by SmartCut method have much higher electron mobility than our samples. However, it has to be mentioned that the electron mobility obtained in the present work was measured for much higher electron concentrations.

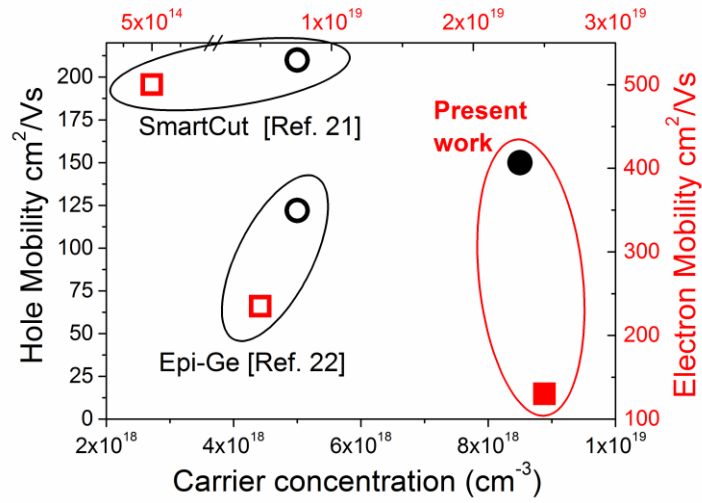


Figure 4. The carrier mobility as a function of carrier concentration measured from 50 nm thick GeOI implanted with Sn (black solid circle) or double implanted with Sn and P (red solid square) after FLA for 3 ms at 55.6 Jcm^{-2} . For comparison, open symbols show the carrier mobility of SmartCut GeOI and GeOI made by epitaxial layer transfer. The red/square symbols are for electrons and the black/circle symbols are for holes.

In the case of our p-type GeOI, the measured hole mobility is similar to that of Epi-GeOI samples but lower than that of SmartCut GeOI layers. This is reasonable since SmartCut technology is well-established and offers the highest quality single-crystalline wafer available on the market at present.

Conclusions

The p-type and n-type 50 nm GeOI wafers were successfully fabricated using PECVD and ms-range FLA. The n-type GeOI was prepared by P implantation and post-implantation FLA. The carrier mobility was significantly enhanced by Sn alloying. The presented method is fully compatible with Si complementary metal-oxide semiconductor (CMOS) technology. The obtained carrier mobility is comparable with the state-of-the-art of GeOI thin films made by more sophisticated method like epitaxial layer transfer or Smart Cut technology.

Acknowledgements

Support by the Ion Beam Center (IBC) at HZDR is gratefully acknowledged. We would like to thank Andrea Scholtz for XRD measurements. This work was partially supported by the German Academic Exchange Service (DAAD) and the Polish Ministry of Science and Higher Education.

References:

1. P. Chaisakul, D. Marris-Morini, J. Frigerio, D. Chrastina, M. Rouifed, S. Cecchi, P. Crozat, G. Isella and L. Vivien, *Nature Photonics* **8**, 482–488 (2014).
2. R. Chau, B. Doyle, S. Datta, J. Kavalieros and K. Zhang, *Nature Materials* **6**, 810 - 812 (2007).
3. Y. Kamata, *Materials Today*, **11**, 30-38 (2008).
4. P. S. Goley and M. K. Hudait, *Materials* **7**, 2301-2339 (2014).
5. <http://www.itrs.net/Links/2013ITRS/Home2013.htm>.
6. A. Nazarov, I. Osiyuk, I. Tyagulskii, V. Lysenko, S. Prucnal, J. Sun, W. Skorupa and R.A. Yankov, *J. Lumin.* **121**, 213 (2006).
7. W. Skorupa, T. Gebel, R. A. Yankov, S. Paul, W. Lerch, D. F. Downey and E. A. Arevalo, *J. Electrochem. Soc.* **152**, G436 (2005).
8. V. Heera, R. Kögler, W. Skorupa and J. Stoemenos, *Appl. Phys. Lett.* **67**, 1999 (1995).
9. S. Prucnal, S. Facsko, C. Baumgart, H. Schmidt, M. O. Liedke, L. Rebohle, A. Shalimov, H. Reuther, A. Kanjilal, A. Mücklich, M. Helm, J. Zuk and W. Skorupa, *Nano Lett.* **11**, 2814 (2011).
10. S. Prucnal, M. Turek, A. Drozdziel, K. Pyszniak, A. Wójtowicz, S. Zhou, A. Kanjilal, A. Shalimov, W. Skorupa and J. Zuk, *Cent. Eur. J. Phys.* **9**, 338-343 (2011).
11. K. Gao, S. Prucnal, R. Huebner, C. Baetz, I. Skorupa, Y. Wang, W. Skorupa, M. Helm and S. Zhou, *Appl. Phys. Lett.* **105**, 042107 (2014).
12. X. Sun, J. Liu, L. C. Kimerling and J. Michel, *Opt. Lett.* **34**, 1198–1200 (2009).

13. S. Wirths, R. Geiger, N. von den Driesch, G. Mussler, T. Stoica, S. Mantl, Z. Ikonik, M. Luysberg, S. Chiussi, J. M. Hartmann, H. Sigg, J. Faist, D. Buca and D. Grützmacher, *Nature Photonics* **9**, 88–92 (2015).
14. N. A. Blum and C. Feldman, *J. Non-Cryst. Solids* **22**, 29 (1976).
15. L. Nikolova, T. LaGrange, B. W. Reed, M. J. Stern, N. D. Browning, G. H. Campbell, J.-C. Kieffer, B. J. Siwick and F. Rosei, *Appl. Phys. Lett.* **97**, 203102 (2010).
16. M. Posselt and A. Gabriel, *Phys. Rev. B* **80**, 045202 (2009).
17. L. Nikolova, T. LaGrange, M. J. Stern, J. M. MacLeod, B. W. Reed, H. Ibrahim, G. H. Campbell, F. Rosei and B. J. Siwick, *Phys. Rev. B* **87**, 064105 (2013).
18. J. H. Parker, Jr., D. W. Feldman, and M. Ashkin, *Phys. Rev.* **155**, 712 (1976).
19. P.Y. Yu, M. Cardona, *Fundamentals of Semiconductors*, Graduate Texts in Physics, 4th ed., © Springer-Verlag Berlin Heidelberg 2010 DOI 10.1007/978-3-642-00710-1_9,
20. J. R. Weber, A. Janotti, and C. G. Van de Walle, *Phys. Rev. B* **87**, 035203 (2013).
21. C. G. Van de Walle and J. Neugebauer, *Nature* **423**, 626-628 (203).
22. V. P. Markevich, A. R. Peaker, B. Hamilton, V. V. Litvinov, Yu. M. Pokotilo, S. B. Lastovskii, J. Coutinho, A. Carvalho, M. J. Rayson and P. R. Briddon, *J. Appl. Phys.* **109**, 083705 (2011).
23. C. H. Lee, T. Nishimura, T. Tabata, D. D. Zhao, R. Ifuku, K. Nagashio, K. Kita, and A. Toriumi, *IEEE Int. SOI Conf.*, p. 1 (2011).
24. X Yu, R. Zhang, J. Kang, T. Maeda, T. Itatani, T. Osada, M. Hata, M. Takenaka and S. Takagi, *ECS Solid State Letters*, **4**, P15-P18 (2015).